doi: https://doi.org/10.2514/1.C034661

Integrated Sizing and Multi-objective Optimization of Aircraft and Subsystem Architectures in Early Design

Dushhyanth Rajaram[a], Yu Cai[a], Imon Chakraborty[b], and Dimitri N. Mavris[c]
Aerospace Systems Design Laboratory, Georgia Institute of Technology, Atlanta, Georgia, 30332-0150.

The aerospace industry's current trend towards novel or More Electric architectures results in some unique challenges for designers due to both a scarcity or absence of historical data and a potentially large combinatorial space of possible architectures. These add to the already existing challenges of attempting to optimize an aircraft design in the presence of multiple possible objective functions while avoiding an overly compartmentalized approach. This paper uses the Integrated Subsystem Sizing and Architecture Assessment Capability to pursue a multi-objective optimization for a Large Twin-aisle Aircraft and a Small Single-aisle Aircraft using the Non-dominated Sorting Genetic Algorithm II with parallel function evaluations. One novelty of the optimization setup is that it explicitly considers the impacts of subsystem architectures in addition to those of traditional aircraft-level design variables. The optimization yielded generations of non-dominated designs in which substantially electrified subsystem architectures were found to predominate. As a first assessment of the impact of epistemic uncertainty on the results obtained, the optimization was re-run with altered sensitivities for the thrust-specific fuel consumption penalties due to shaft-power and bleed air extraction. This analysis demonstrated that the composition of architectures on the Pareto frontier is sensitive to the secondary power extraction penalties, but more so for the Small Single-aisle Aircraft than the Large Twin-aisle Aircraft.

[a] Graduate Research Assistant, Daniel Guggenheim School of Aerospace Engineering, AIAA Student Member.
[b] Research Engineer II, Daniel Guggenheim School of Aerospace Engineering, AIAA Member.
[c] S.P. Langley NIA Distinguished Regents Professor, Daniel Guggenheim School of Aerospace Engineering, AIAA Fellow.

This paper was presented on June 5, 2017 as paper # AIAA 2017-3067 at the AIAA AVIATION Forum and Exposition 2017, Denver, CO, June 5-9, 2017.

I. Introduction

The goal of the aircraft sizing task is to use relevant point performance and mission performance requirements to iteratively arrive at a converged solution where the aircraft is defined by a geometric scale (typically represented by wing planform area), a propulsive scale (typically represented by rated sea-level static thrust), and the Maximum Takeoff Weight (MTOW). Thus, the early design phase is dominated by considerations of aerodynamics, propulsion, and structural weight estimation.

Design optimization is typically pursued by posing an optimization problem with appropriate design variables and applicable constraints related to geometry, point performance, and mission performance. Thoroughly adequate (if not optimal) performance must be ensured with respect to multiple, often conflicting, performance objectives. In addition to the obvious objective of minimizing fuel consumption, other common choices seen in literature [1–5] include MTOW (often used as a surrogate for cost), Operating Empty Weight (OEW) NO_x, CO_2 emissions, takeoff field length, specific range (a surrogate for off-design fuel economy), design range, noise margin, etc. This results in a fundamentally multi-objective optimization problem, where the conflicting nature of the objectives may preclude the existence of designs that are optimal with respect to all objectives. In such cases, rather than a single optimal design, a set of *non-dominated Pareto-optimal* solutions is sought, whose members are considered equally good, and for whom no single objective can be further improved without degradation of one or more other objectives.

Design variables for such optimization problems are typically at the aircraft-level and relate to geometric, aerodynamic, and propulsive characteristics. However, the aerospace industry's current trend towards *More Electric Aircraft* (MEA) [6–8], driven by rapidly improving state-of-the-art in power electronics and electric drives [9, 10], adds the vehicle's subsystem architecture to the optimization problem as additional *discrete* degrees-of-freedom. As enumerated in prior work [11], multiple possible solutions for multiple subsystems can lead to a very large number of combinatorial possibilities. Historical data for such unconventional architectures is limited or absent, and existing regression relationships based off historical data [12–14] may be inapplicable, since they were developed from the decades-long persistence of a fairly conventional subsystems architecture: pneumatic Environmental Control System (ECS) and Ice Protection Systems (IPS), hydraulic actuation func-

tions, and electrically powered avionics and cabin loads. Thus, accounting for the non-negligible impact of novel subsystems architecture requires explicit consideration of subsystems earlier in the design phase, possibly through physics-based sizing and analysis approaches [15–17], and accounting for the connectivity among various components within the subsystem architecture.

First among the salient features of this work is the use of the Non-dominated Sorting Genetic Algorithm II (NSGA-II) [18] for optimization. Genetic Algorithms in general are inherently suited to optimization problems involving discrete design variables (e.g., subsystem architecture descriptions) and large design spaces. Due to the presence of a small degree of randomness owing to their evolutionary nature, they are known to capture the global minimum if run indefinitely. In addition, because they do not rely on gradient information, they can handle highly nonlinear, discontinuous functions. This makes them especially suitable when harnessing engineering design codes where the underlying analytical relationships may be unknown, complex, and/or implicit. The NSGA-II algorithm, in particular, is ideally suited to multi-objective optimization. It employs a fast, non-dominated sorting approach and has been shown to be capable of finding a better spread of solutions with better convergence near a Pareto front compared to other algorithms [19].

Second, this work uses the Integrated Subsystem Sizing and Architecture Assessment Capability (ISSAAC) framework [16, 20, 21] to explicitly assess the impact of subsystems architecture on airplane sizing and performance. The ISSAAC framework integrates a tractable, physics-based sizing and analysis of major aircraft subsystems with the traditional aircraft sizing process in a modular manner, with a focus on novel architectures (e.g., MEA). In this work, the NSGA-II algorithm supplies both aircraft-level continuous design variables and discrete subsystem-level architecture descriptor variables to the ISSAAC framework, which evaluates and returns the candidate design's performance with regard to the objective functions and constraints. The end goal of this optimization approach is to identify the characteristics of the Pareto-optimal designs, with regard to both the continuous (aircraft-level) and discrete (subsystem-level) design variables for a Large Twin-Aisle Aircraft (LTA) and a Small Single-Aisle Aircraft (SSA). Some of these insights are not observable from conventional sizing/analysis methods and optimization setups unless the subsystems architecture of the aircraft is explicitly taken into account.

Third, since the results of any trade studies are affected by epistemic uncertainty, conclusions from the optimization results are drawn based on architectures present within a look-back region, rather than based solely on the Pareto frontier of the final generation of the GA. Further, populations obtained with multiple settings of a parameter controlling GA crossover are considered, in order to increase robustness with respect to the non-deterministic behavior of the algorithm.

The remainder of the paper is organized as follows: Section II gives a brief description of the characteristics of the NSGA-II algorithm which is employed in this work. Section III gives a brief summary of the ISSAAC framework, which in this case is driven by the NSGA-II algorithm. Section IV discusses the proposed approach and the problem formulation. Section V presents and discusses the results of the optimization. Section VI concludes the paper and identifies some avenues for future work.

II. Non-dominated Sorting Genetic Algorithm II (NSGA-II)

Several algorithms exist for computing the Pareto frontier [22–24] and popular approaches are evolutionary in nature [18]. Some popular non-evolutionary approaches include (but are not limited to) normal boundary intersection [24] and normal constraint based methods [22, 23]. These methods involve solving a set of single objective optimization problems usually involving a weighted-sum of the objectives to successively sample points on the Pareto frontier. Approaches that operate on such weighted-sum aggregates are known to be inappropriate for determining non-convex regions on the Pareto frontier and struggle to attain an evenly spaced distribution of points [24]. The NSGA-II algorithm employed herein works much like genetic algorithms, in that it operates on a "population" of candidate designs, and successively returns populations that are non-dominated until a convergence criterion is met. Common genetic operators like cross-over (reproduction), mutation, and selection ensure that as generations progress, fitter members of the population are retained while the poorly performing members get discarded. In the multi-objective setting, a notion of the existence of non-domination levels in the population helps in the retention of the most non-dominated members as time advances. In other words, the members that are most non-dominated replace older members in the population. Constraint violations can be handled in a number of ways. In this work, constraints are handled by penalizing the dominance level of the population member

in question in an adverse manner that guarantees that it does not emerge on the Pareto frontier. Another important feature of the NSGA-II algorithm that is particularly relevant to this work is the fact that it naturally lends itself to parallelization because it requires that a set of candidates be evaluated at any given point in time. This set of designs can therefore be evaluated simultaneously in parallel.

III. Integrated Subsystem Sizing and Architecture Assessment Capability (ISSAAC)

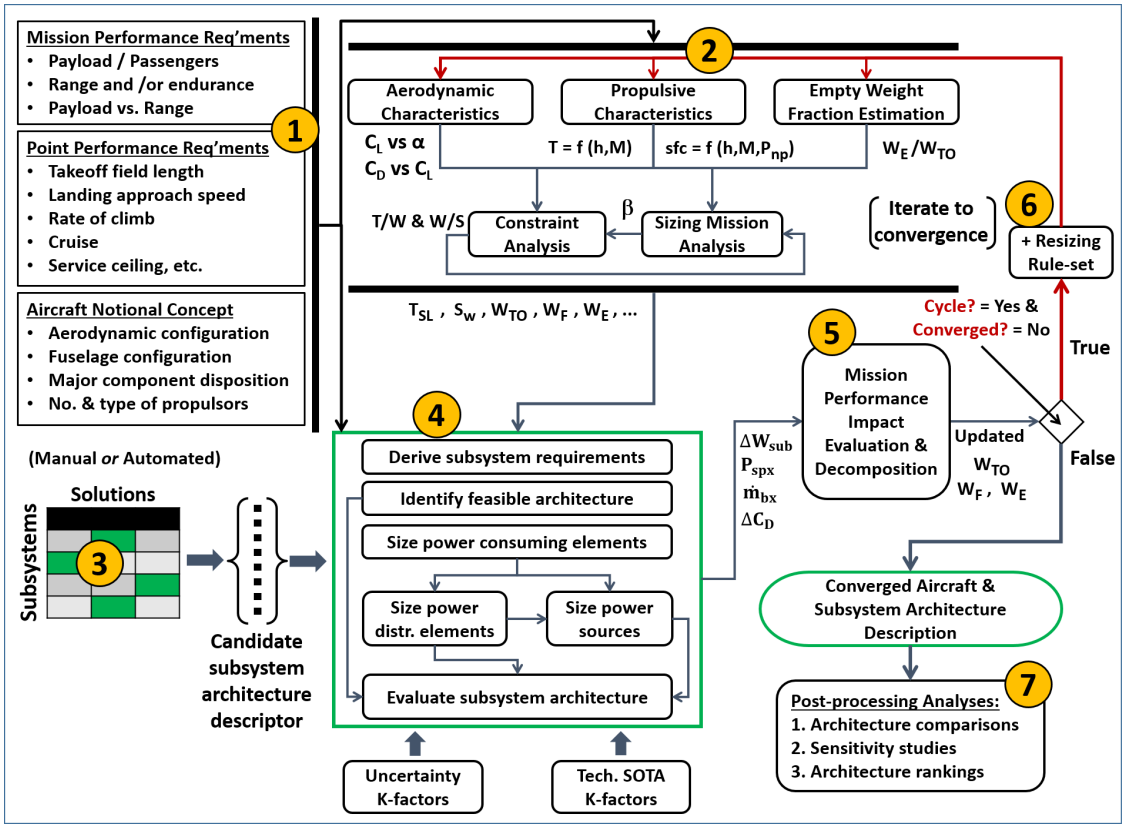

Fig. 1 Main modules of Integrated Subsystem Sizing and Architecture Assessment Capability (ISSAAC)

This section provides a brief summary of the main modules of ISSAAC, which are depicted in Fig. 1. For additional details, the reader is referred to prior works involving ISSAAC [16, 20, 21]. It requires the integration of tools possessing the following functionalities or capabilities (listed in parentheses are the tools currently used in ISSAAC):

1. Aircraft sizing and mission performance analysis (Flight Optimization System (FLOPS) [25])

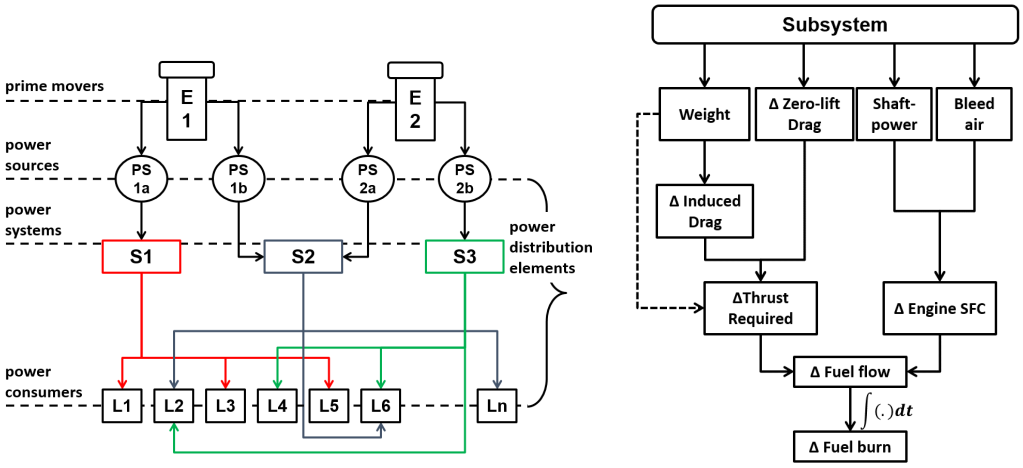

(a) Generalized representation of subsystems architecture

(b) Impact of subsystems on fuel consumption (mission-level metric)

Fig. 2

2. Propulsion cycle analysis (Numerical Propulsion System Simulation [26])

3. Subsystem sizing and analysis capability (MATLAB)

4. Analysis module integration and sequencing (MATLAB)

The main ISSAAC modules (shown depicted in Fig. 1) involve:

1. **Definition of design requirements:** These include the mission performance requirements (e.g., design range and payload), the point performance requirements (e.g., takeoff field length, approach speed, etc.), and the aircraft notional concept.

2. **Traditional aircraft & engine sizing:** This module uses FLOPS to size the aircraft based on the design mission. FLOPS weight relationships for subsystems are based on regressions of historical data, and therefore apply to conventional architectures. These starting estimates are subsequently overridden by calculations performed in Module 4.

3. **Candidate subsystem architecture descriptor:** This provides a qualitative description of the design solutions for each subsystem to be evaluated. Subsystems considered in this work include ECS, wing IPS (WIPS), cowl IPS (CIPS), and a number of actuation functions.

4. **Subsystem architecture sizing and evaluation:** This module sizes the major elements within the subsystem architecture (Fig. 2(a)). It computes weight, secondary power require-

ments (shaft-power or bleed air), and direct drag increments. The latter three time-varying quantities are computed for each subsystem and also for the architecture as a whole.

5. **Mission performance impact evaluation and decomposition:** This module evaluates the impact of subsystems architecture weight, secondary power requirements, and drag increments (Fig. 2(b)) on aircraft mission performance, e.g., fuel consumption and gross weight. Both the cumulative effect and the individual contributions from each subsystem are tracked.

6. **Re-sizing of aircraft & subsystems:** This module re-sizes the aircraft and its subsystems in accordance with certain re-sizing rules. In this work, the aircraft is re-sized to maintain the thrust-to-weight ratio (T_{SL}/W_{TO}) and wing loading (W_{TO}/S_w) supplied by the optimizer (described in Sec. IV A). The design range and cruise Mach number are also held fixed. Additionally, constant stabilizer volume ratios are imposed (representing invariant stability and control requirements). The module terminates when changes in the vehicle gross weight and subsystem weights between successive iterations are each smaller than a specified tolerance.

7. **Post-processing analyses:** This is a customizable module depending on the type of analysis being performed. In this work, they include plots depicting the Pareto frontier and its architectural constitution for successive generations, as well as the variation of continuous aircraft-level and discrete subsystem-level design variables within a look-back region.

The propulsion cycle sizing and analysis tool (NPSS) is not currently directly embedded within ISSAAC. Instead, it is run off-line to generate engine performance data tables (engine decks) that are then used for sizing and mission performance analysis within the ISSAAC framework. Further, currently there is no computation of aircraft acquisition or operating costs.

A. Brief Overview of ISSAAC Subsystem Modules

The subsystems considered within ISSAAC are divided into two groups, as shown in Fig. 3, which are evaluated in the following order:

1. Power consuming subsystems: which consume secondary power in pneumatic, hydraulic, or electric form and provide necessary functionality to the aircraft.

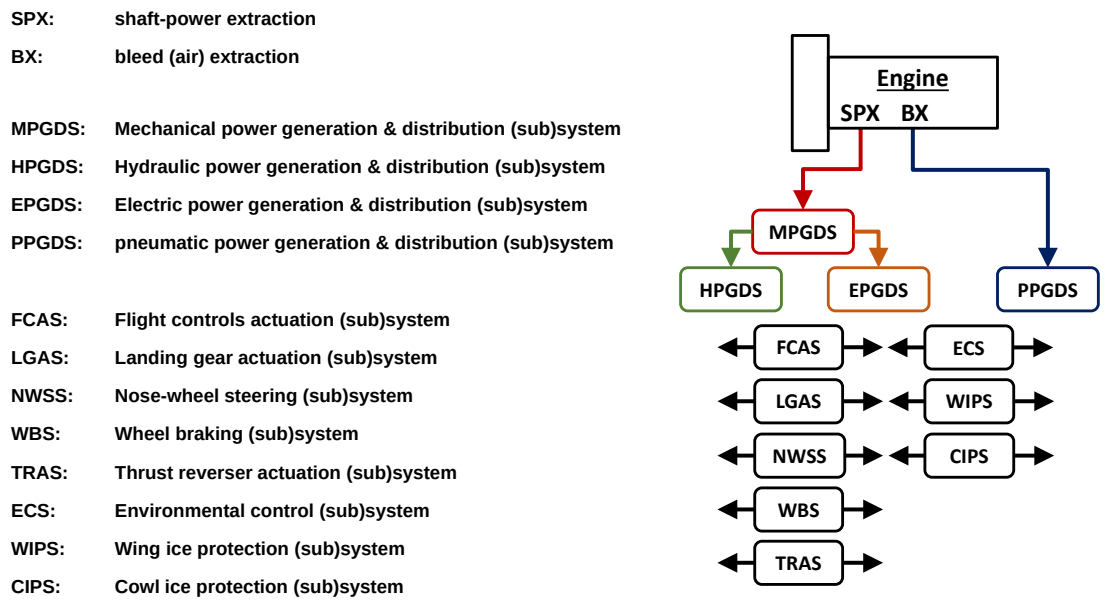

Fig. 3 ***Power consuming*** **and** ***power generation and distribution*** **subsystems considered**

2. Power generation and distribution subsystems: which are responsible for generation of secondary power, its transformation/regulation, and its distribution to the power consumers.

For each subsystem considered, the end goal of the modeling approach is to identify the impacts along the four avenues shown in Fig. 2(b): (i) weight w_{sub}, (ii) shaft-power requirement $P_{spx}(t)$, (iii) bleed air requirement $\dot{m}_b(t)$, and (iv) direct drag increment $\Delta C_D(t)$ (the latter three may or may not be present, depending on the subsystem).

The connectivity among prime movers, power sources, power systems, and power consumers within an architecture (Fig. 2(a)) is determined automatically by an architecture definition algorithm. Using heuristic rules identified from inspection and extrapolation of the subsystem architectures of existing conventional aircraft and MEA, this algorithm rapidly determines a feasible connectivity among architecture components. Prior work [27] showed this to be equivalent to (or more conservative than) those present in existing commercial aircraft from a redundancy standpoint.

The Flight Controls Actuation System (FCAS) uses flight control surface definitions that are relative to the lifting surfaces. Sizing actuation loads for hinged control surface (ailerons, elevators, rudder, and spoilers) are computed using hinge moment coefficients [28] and relevant constraining flight conditions [29, 30]. Actuating power requirements within a mission are estimated using the

Table 1 Definition of Actuation Function Packages (AFPs) for FCAS, LGAS, NWSS, WBS, & TRAS

Actuation Function	Actuation Function Package (AFP) # (Electrification indicated by ✓or electric actuator type)							
	AFP-0	AFP-1	AFP-2	AFP-3	AFP-4	AFP-5	AFP-6	AFP-7
TRAS		✓	✓	✓	✓	✓	✓	✓
WBS		✓	✓	✓	✓	✓	✓	✓
LGAS			✓	✓	✓	✓	✓	✓
NWSS			✓	✓	✓	✓	✓	✓
FCAS-HLD				✓	✓	✓	✓	✓
FCAS-Sp.				EHA	EMA	EMA	EMA	EMA
FCAS-THSA					✓	✓	✓	✓
FCAS-Prim.						H/EHA	EHA	EMA

Acronyms & Abbreviations - EHA: electrohydrostatic actuator, EMA: electromechanical actuator, H/EHA: hydraulic actuator & EHA in parallel, HLD: high-lift devices, THSA: trimmable horizontal stabilizer actuator, Sp.: spoilers, Prim.: primary flight control surfaces

hinge moment coefficients and assumed control surface duty cycles [31]. Actuating power requirements for the high-lift devices and trimmable horizontal stabilizer are estimated using relationships between these quantities and aircraft maximum takeoff mass that were developed using published data for existing aircraft [17, 32–34]. Estimates of the mass properties of the landing gears and a simplified model of the retraction/extension kinematics [35] are used to compute the actuation requirements for the Landing Gear Actuation System (LGAS). Nose-wheel Steering System (NWSS) actuation power requirement is computed based on gear geometry and critical loading conditions that generate maximum steering moments [35, 36]. Predicted loads showed reasonable agreement with published loads from the ELGEAR project [37] (for Airbus A320 aircraft). Wheel Braking System (WBS) actuation requirements are computed using constraining static and dynamic braking cases [30, 35, 38]. Thrust reverser power requirements are expressed using a relationship that relates required power linearly to rated sea-level static engine thrust, which was developed using

limited available data [34, 39]. For each of these systems, the hydraulic or electric actuator masses are determined based on the actuation load/power that they are sized for. The presence of multiple actuation functions and multiple actuator designs results in a very large number of overall actuation architecture possibilities. Considering both computational tractability and the industry's demonstrated conservatism regarding electrification of actuation functions, it is assumed that they are electrified in a staged or *packaged* approach through a limited number of *Actuation Function Packages* (AFPs) AFP-0,..., AFP-7, as shown in Table 1. The successive actuation packages AFP-0, ..., AFP-7 involve electrification of progressively more flight-critical actuation functions.

The ECS power requirement and drag generation are estimated based on (i) a cabin thermal analysis that accounts for internal heat loads and heat transfer between the cabin and the ambient across the cabin wall and (ii) a thermodynamic model of the ECS pack to compute the required mass flow rate of cooling ram air. To reduce case run time, the pack thermodynamic model is first evaluated off-line in order to create a gridded interpolant that relates required ram air mass flow with flight condition, pack air entry condition, and pack discharge temperature. This meta-model (and not the original pack model) is then queried during the mission performance evaluation. For electric ECS, mass additions from the cabin air compressors, electric motors, and their associated power electronics (which are driven by the electric pressurization power requirements) are accounted for [20]. Predicted power requirements compared well with published estimates for electric pressurization [40], when reduced to a power-per-occupant basis.

The heating requirements for the Wing Ice Protection System (WIPS) and Cowl Ice Protection System (CIPS) are computed based on the protected surface area (defined parametrically with respect to the parent surface, i.e., the wing or the nacelle) and the necessary heat flux for a given flight and atmospheric condition [20]. These are computed using only limited geometric information about the aircraft's protected area. However, it was shown by other authors [41] that even such an approach provided acceptable estimates of the IPS power requirements for the Boeing 787 aircraft. The IPS mass is computed using a mass/length figure for pneumatic IPS and a mass/area figure for electrothermal IPS.

For hydraulic, pneumatic, and electric power generation and distribution systems (HPGDS,

PPGDS, and EPGDS respectively), the masses of the power distribution elements (respectively hydraulic pipes, pneumatic ducts, and electric cables) are computed by (i) determining their existence and lengths from the architecture connectivity and the geometric model of the aircraft, and (ii) determining the mass-per-unit-length based on consideration of pressure drop, pressure, and voltage drop respectively. For the HPGDS and EPGDS, power sources (hydraulic pumps and electric generators respectively) are sized through the identification of constraining flight conditions that require the maximum output from these components [20]. Their masses are then calculated from power-to-mass ratios identified from product data-sheets.

IV. Developed Approach

A. Formulating the Optimization Problem

In this work, the problem of simultaneously sizing and optimizing the aircraft and also sizing some major subsystems is posed as a multi-objective optimization statement. As mentioned previously, a number of objectives or objective functions have been considered in prior optimization studies in literature, the choice largely depending on the specific goals of the studies. Since the goal of this work is to analyze the effect of novel subsystem architectures on aircraft performance, two sets of objective functions are considered: (i) *take-off field length* (TOFL) and *block fuel* (BF) and (ii) *operating empty weight* (OEW) and *block fuel*. Take-off field length may be viewed as a surrogate for airport accessibility, and therefore is of interest to commercial airline carriers. Block fuel, on the other hand, is an indicator of fuel efficiency for a given design range. Finally, for a given MTOW, a lower OEW implies a greater useful load capacity (payload and fuel). The rationale for choosing only two objectives is to simplify visualization and comparison of designs on different Pareto fronts.

The choice of design variables in a conceptual design study is usually motivated by the following: (i) designers should have access to them, and (ii) they should affect the aerodynamics, propulsion, and structures disciplines in an obvious, estimable, and significant manner. Thus, thrust-to-weight ratio (TWR), wing loading (WSR), wing quarter chord sweep (SWEEP), wing thickness-to-chord ratio (TCA), wing taper ratio (TR), and wing aspect ratio (AR) are chosen as the aircraft-level design variables. These are continuous design variables, which may take any value within defined upper and lower bounds (shown in Table 2).

The subsystem architectures, on the other hand, are described by discrete design variables (shown in Fig. 4) that denote the overall solutions employed for each subsystem. The first digit represents the Actuation Function Package (AFP), described in Table 1. The second and third digits describe the WIPS and CIPS solutions. These may differ in the secondary power type used

Table 2 Continuous and discrete design variable ranges

	Range	
Design Variables	**SSA**	**LTA**
Thrust-to-weight ratio (TWR)	[0.25, 0.35]	[0.25, 0.35]
Wing loading (WSR, lb/ft^2)	[120, 135]	[115, 135]
Quarter-chord sweep (SWEEP, deg)	[25, 40]	[30, 40]
Thickness-to-chord ratio (TCA)	[0.05, 0.13]	[0.05, 0.13]
Taper ratio (TR)	[0.1, 0.4]	[0.1, 0.4]
Aspect ratio (AR)	[8, 12]	[10, 15]
Actuation function package (AFP)	{0, 1, . . . , 7}	{0, 1, . . . , 7}
Wing ice protection system (WIPS)	{0, 1, 2, 3}	{0, 1, 2, 3}
Cowl ice protection system (CIPS)	{0, 1, 2, 3}	{0, 1, 2, 3}
Environmental control system (ECS)	{0, 1}	{0, 1}

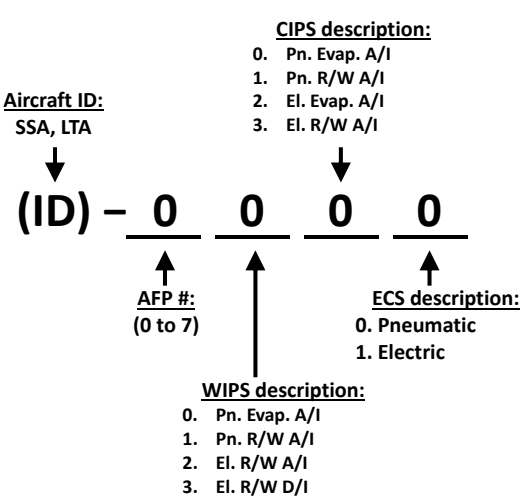

Fig. 4 Subsystem architecture descriptor featuring discrete design variables

(pneumatic vs. electric), the magnitude of supplied heat flux (in evaporative systems, the heat supplied is sufficient to completely evaporate impinging water, unlike in running-wet systems), and in the mode of operation (anti-ice systems operate continuously to prevent ice formation, while de-ice systems activate periodically to dispatch ice buildup). The fourth digit describes whether the ECS is of a conventional pneumatic type, which uses bleed air from the engines for cabin pressurization, or an electric solution which uses electrically driven compressors to compress ram air. Table 2 shows the discrete values that the subsystem architecture descriptor variables may take.

In modern-day aircraft design programs, it is not uncommon for airframers to sub-contract the design of major aircraft subsystems to vendors and suppliers. Thus, while the airframers may be in a position to evaluate the effect of entirely different subsystem architectures, they may not be able to adequately address the detailed design of these subsystems. Therefore, while additional continuous design variables related to the detailed design and optimality of the subsystems clearly do exist, these are not considered within the scope of the current work.

The optimization is subject to the following constraints, each of which is cast as an inequality constraint: (i) maximum TOFL (7,500 ft for both SSA and LTA), (ii) maximum wingspan (118 ft for SSA, 214 ft for LTA), (iii) positive excess fuel capacity, (iv) positive excess thrust (thus, climb gradient) for one-engine inoperative missed approach (AMFOR) (v) positive excess thrust (thus, climb gradient) for one-engine inoperative second segment climb (SSFOR), and (vi) maximum landing approach speed ($\mathrm{VAPP}_{\mathrm{max}}$, 150 kt for both SSA and LTA). The positive excess thrust for one-engine inoperative second segment climb (SSFOR) and positive excess thrust for one-engine inoperative missed approach (AMFOR) constraints place lower bounds on permissible thrust-to-weight ratio, while the upper-bound on permissible landing approach speed constrains maximum feasible wing loading. The upper-bound on wingspan constrains the feasible aspect ratio for a given wing area. The fuel volume constraint effectively imposes a lower bound on feasible thickness-to-chord ratio of the wing for a given wing area. It should be noted that the optimization framework developed is easily amenable to the inclusion of such additional constraints.

Side constraints representing the upper and lower bounds of continuous design variables and permissible values of discrete design variables are listed in Table 2. The optimization problem may

now be formally stated as follows:

$$
\begin{aligned}
\underset{\mathbf{x}}{\text{minimize}} \quad & \mathbf{f}(\mathbf{x}) = \begin{bmatrix} \text{TOFL}(\mathbf{x}) \\ \text{BF}(\mathbf{x}) \end{bmatrix} \quad \text{or} \quad \begin{bmatrix} \text{OEW}(\mathbf{x}) \\ \text{BF}(\mathbf{x}) \end{bmatrix} \\
\text{subject to} \quad & \text{TOFL}(\mathbf{x}) - \text{TOFL}_{\text{baseline}} \leq 0, \\
& \text{Span}(\mathbf{x}) - \text{Span}_{\text{max}} \leq 0, \\
& \text{Required fuel}(\mathbf{x}) - \text{Fuel capacity}(\mathbf{x}) \leq 0, \\
& -\text{AMFOR}(\mathbf{x}) \leq 0, \\
& -\text{SSFOR}(\mathbf{x}) \leq 0, \\
& \text{VAPP}(\mathbf{x}) - \text{VAPP}_{\text{max}} \leq 0, \\
& \mathbf{x} : [\text{TWR, WSR, SWEEP, TCA, TR, AFP, WIPS, CIPS, ECS}]^T \in [\text{Table 2 intervals}]
\end{aligned}
$$

As the optimizer varies the design variables during the optimization, there may be combinations of design variables that fail to yield converged designs or result in errors thrown by ISSAAC modules (typically originating from FLOPS). Such situations, once detected, are handled by artificially appending high values to the objective functions (orders of magnitude higher than those for converged cases). This ensures that such designs are not carried forward into subsequent generations. Rather than finding a single optimum, the aim of this multi-objective optimization is to obtain Pareto-efficient designs in terms of the chosen objectives.

B. Optimization Workflow

To perform the optimization described in the preceding section, the ISSAAC framework was integrated with MATLAB's NSGA-II algorithm with the input/output interfaces depicted in Figure 5. The NSGA-II algorithm generates combinations of design variables (both continuous aircraft-level variables and discrete subsystem architecture descriptors) and queries ISSAAC, which performs the aircraft and subsystem sizing as well as the mission performance evaluation and returns values of the objectives and constraints to the optimization algorithm that correspond to the design variables.

On average, one evaluation costs $\mathcal{O}(40)$ seconds on a 3.40 GHz Intel i7 CPU with 16 GB of DDR3 RAM. For a high number of function calls (typically the case for evolutionary optimizers), this

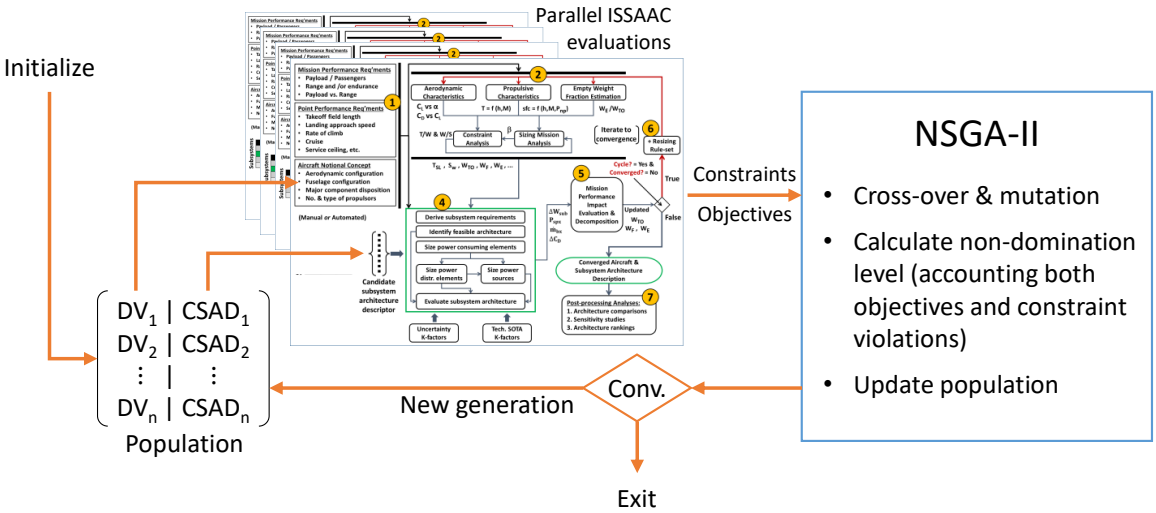

Fig. 5 Optimization workflow depicting interfaces between the NSGA-II optimizer and the ISSAAC framework

can result in intractable run times. Therefore, in order to reduce run time, queries to ISSAAC are parallelized. Thus, when the optimizer requires a set of candidates to be evaluated to determine their objectives and constraints, the work is split into different *workers* (processes), enabling simultaneous independent evaluations.

C. Establishing Reference Conventional Architecture Designs

To assess the effect of subsystem architectures on aircraft performance, two aircraft sizes are considered: (i) Small Single-aisle Aircraft (SSA) - similar to the Boeing 737-800, (ii) a Large Twin-aisle Aircraft (LTA) - similar to the Boeing 787-8. For both the aircraft classes, an optimization is first performed over only the aircraft-level continuous design variables with the subsystem architecture descriptors set to a conventional architecture (i.e., SSA-0000 and LTA-0000, see Fig. 4). The objective of this smaller-scale optimization problem is to establish a reference Pareto frontier to facilitate relative comparison of other subsystem architectures. From this Pareto frontier, the utopia point, defined as the hypothetical point that has the minimum of both objectives, is identified. Then, the design on the Pareto frontier that is closest to the utopia point (in the space of objectives) is chosen as a reference design. Since the objectives are physically different quantities, they are first normalized by their range prior to distance (norm) computations for all designs on the reference Pareto frontier. Figure 6 shows a graphical representation

Table 3 Data summary for reference Small Single-aisle Aircraft (SSA-0000) and Large Twin-aisle Aircraft (LTA-0000)

	Aircraft Identity	
Aircraft data	**SSA**	**LTA**
Passenger capacity	160	242
Design range (NM)	3,140	7,355
Cruise Mach number	0.780	0.850
Sea-level static thrust (lbf)	2 x 28,406	2 x 78,839
Wing planform area (ft^2)	1,411	4,061
Wingspan (ft)	118.0	217.4
Wing taper ratio	0.104	0.103
Wing 1/4-chord sweep (deg)	27.7	36.5
HT planform area (ft^2)	361	740
HT aspect ratio	6.27	5.22
HT taper ratio	0.203	0.243
HT 1/4-chord sweep (deg)	29.9	36.6
VT planform area (ft^2)	296	497
VT aspect ratio	1.92	1.80
VT taper ratio	0.276	0.327
VT 1/4-chord sweep (deg)	35.0	40.6
Fuselage length (ft)	124.8	183.4
Fuselage max. width (ft)	12.3	18.9
Fuselage max. height (ft)	13.2	19.4

of the procedure used to establish the reference SSA and LTA designs (summarized in Table 3) and corresponding objective function values BF_{ref} and TOFL_{ref}. The BF and TOFL performance of all designs are expressed subsequently as percentage-deltas (%Δ), which are computed as $\%\Delta\mathrm{BF} = 100 \cdot (\mathrm{BF} - \mathrm{BF}_{ref})/\mathrm{BF}_{ref}$, $\%\Delta\mathrm{TOFL} = 100 \cdot (\mathrm{TOFL} - \mathrm{TOFL}_{ref})/\mathrm{TOFL}_{ref}$.

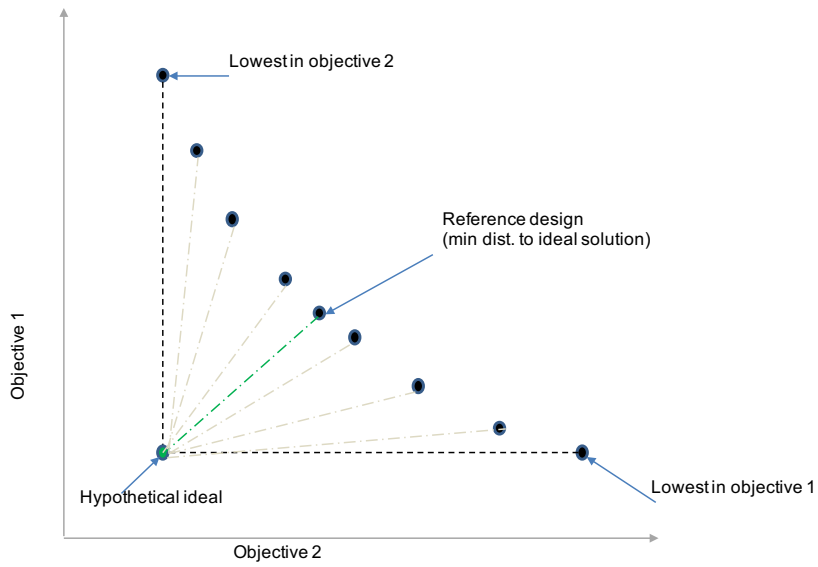

Fig. 6 Visualization of the reference baseline

V. Results

A. NSGA-II Settings

For the smaller-scale optimization problem used to establish the reference SSA-0000 and LTA-0000 designs, a population size of 80 was used. For the larger-scale optimization with all continuous and discrete design variables, a population size of 100 was used. It was found that the choice of a population size of 80-100 members for optimization resulted in a dense enough sampling on the Pareto frontier. Higher population sizes increased the computational cost without any additional benefit in the quality of solution obtained for the purposes of this study. The crossover function permits setting a parameter ranging between 0 and 1 that decides the extent of crossover between design candidates (higher values result in higher extent of crossover). Each optimization problem instance was run with three settings (low, mid, and high) of the crossover parameter. The resulting solutions from each were then combined using a Pareto filter applied on the union of the respective Pareto frontier sets. For mutation, an adaptive feasible mutation function was used that introduces

randomness in design members in a feasible direction while ensuring that the resulting design is feasible. This requirement does not permit setting any factor that introduces uncertainty in the results except for the inherent nature of the mutation operator itself. The optimization runs converged when the average change in the value of the spread of solutions over 100 generations reached a value less than 10^{-4} and the final spread reached a value less than the average spread over the past 100 generations. All the points are retained on the converged Pareto frontier. However, to ensure that they are truly non-dominated, the final population of designs is subject to a Pareto filter. The results are discussed in the following sections.

B. Small Single-Aisle Aircraft (SSA)

Figure 7 shows the movement of the SSA TOFL, BF optimization's Pareto frontiers and also the composition of subsystem architectures (in percentages) with successive generations. The magnitude of improvement between generations (with respect to the BF and TOFL objective functions) reduces significantly as the optimization progresses. An interesting observation is the fact that electric ECS solutions (ECS descriptor = 1) feature in 100% of the populations from very early generations onward. This is due to the fact that despite the increased shaft-power off-takes and component mass for electric ECS, the elimination of bleed air off-takes results in a net fuel burn benefit. At roughly the 80th generation mark, the WIPS solution converges to electrothermal running-wet de-icing system (WIPS descriptor = 3), while the CIPS converges to a pneumatic running-wet anti-icing solution (CIPS descriptor = 1). For the actuation functions, the last 30 generations show a roughly constant majority of designs with AFP#-2 (electric actuation for TRAS, WBS, LGAS, and NWSS).

It should be noted that the sizing problems at both the aircraft and subsystem levels are subject to epistemic uncertainty, and furthermore the subsystem-level problem is greatly affected by assumptions regarding technological state-of-the-art. Conclusions based solely on the characteristics of the final generation's Pareto frontier must, therefore, be avoided. Figure 8 shows the variation of both continuous and discrete design variables over a *Pareto band*, which includes the final generation's Pareto frontier as well as designs from prior generations which are not significantly worse-performing. The Pareto band in question was created using a 0.2% "look-back" for both the BF and TOFL and BF and OEW objective function sets. This plot also shows the final Pareto

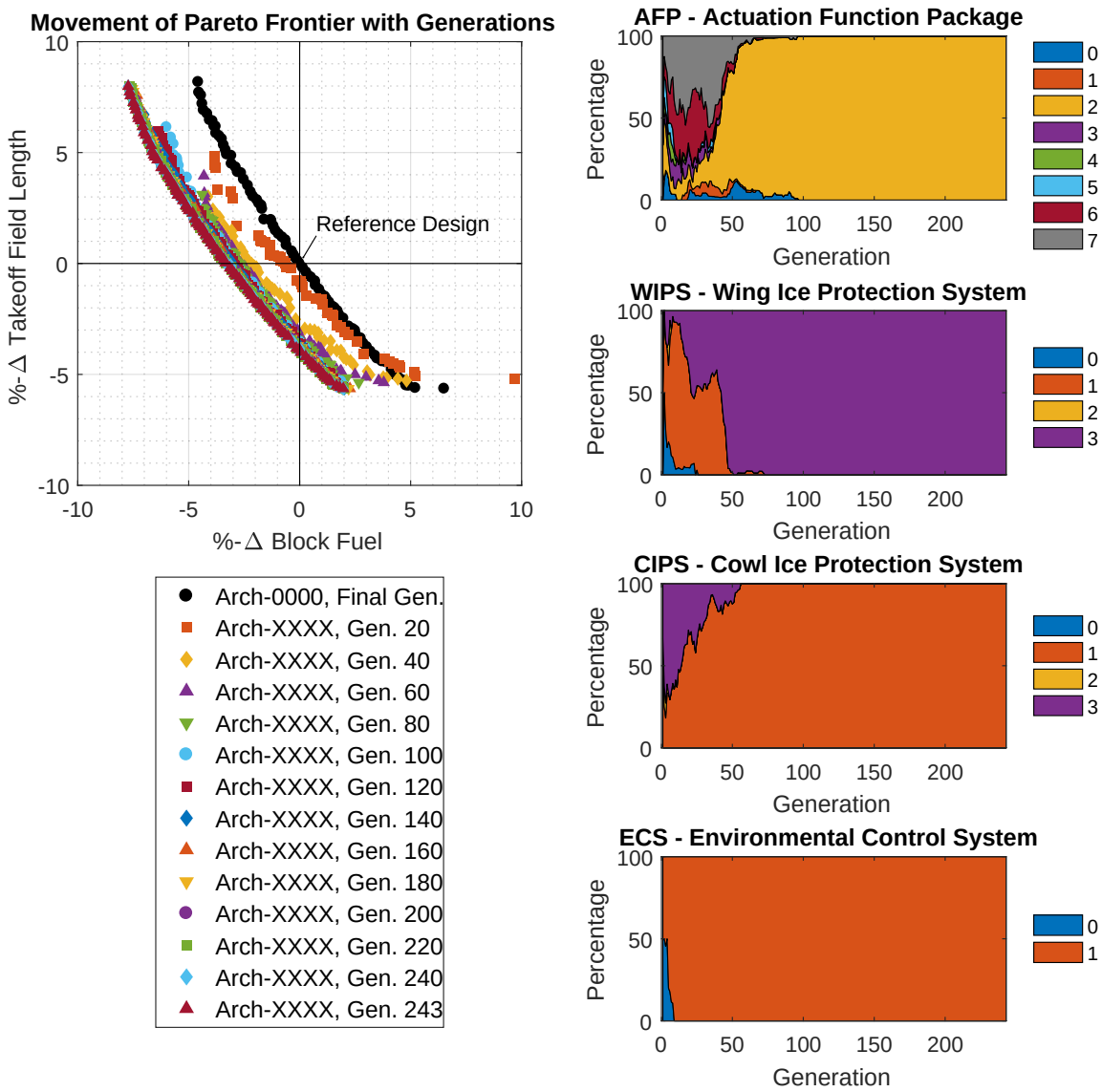

Fig. 7 Evolution (over generations) of SSA BF, TOFL, and architecture compositions on Pareto Frontiers

frontier and the continuous design variable values for the converged conventional architecture, in order to better visualize the impact of including novel electric subsystem architectures. It is evident that designs with higher thrust-to-weight ratio (TWR) perform better with respect to TOFL but worse with respect to BF. Higher aspect ratio (AR) designs also perform better with respect to BF. Within the Pareto band, the variation of the remaining continuous design variables is insignificant i.e. the set of optimal solutions has minor variations in those design variables.

The trends observed with regard to composition of subsystem architectures within the Pareto

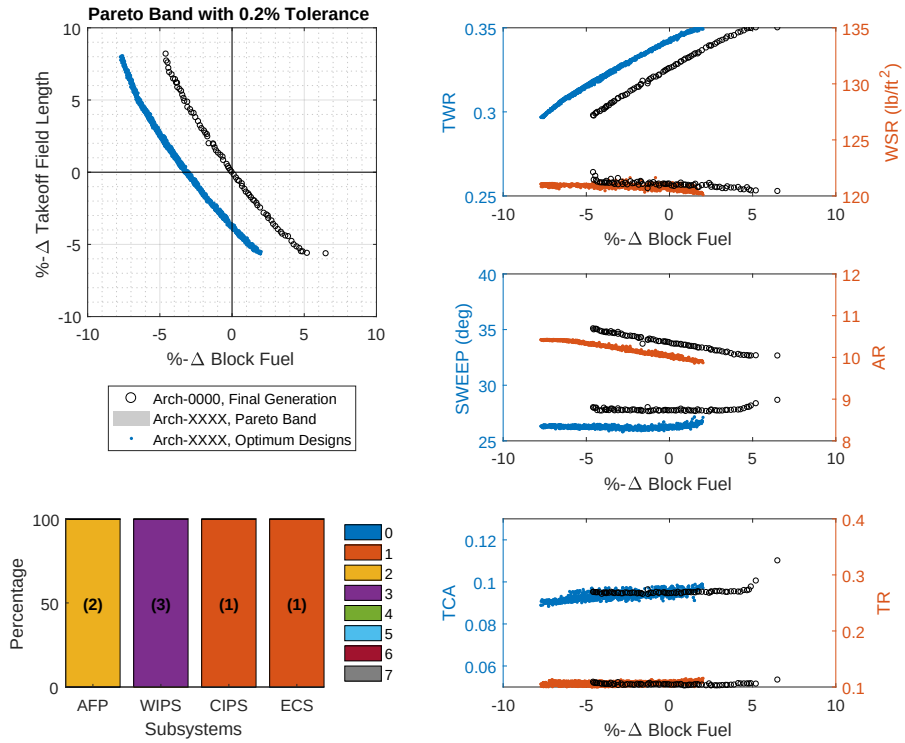

Fig. 8 Variation of SSA TOFL, BF, and design variables within Pareto band

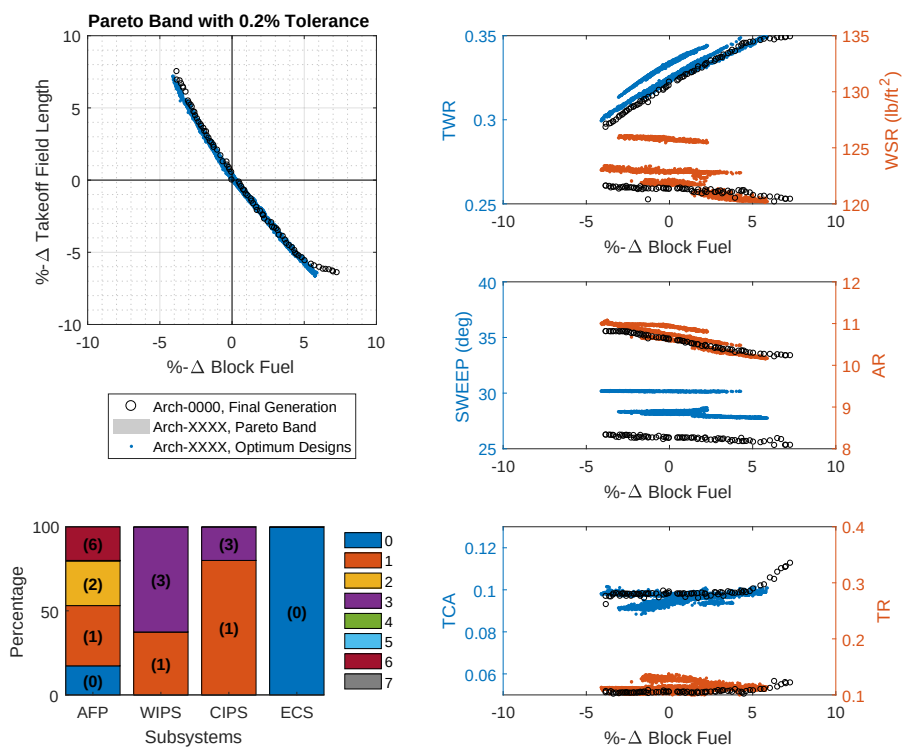

Fig. 9 Variation of SSA TOFL, BF, and design variables within Pareto band, $\kappa_{spp} = 0.5$

band are strongly influenced by the modeling of the thrust-specific fuel consumption (TSFC) penalties arising out of shaft-power and bleed air extraction, which are dependent on the engine cycle parameters. However, in the current approach, the secondary power extraction penalties are estimated using a simpler approach where the incremental fuel flow $\Delta\dot{w}_{f,spx}$ per engine due to total shaft-power extraction of P_{spx} is modeled based on the k_p^* approach of Scholz [42] as

$$\Delta\dot{w}_{f,spx} = \dot{w}_{f,0}\ k_p^*\ \frac{P_{spx}[kW]}{N_{op,eng}\ T_{SL}[kN]}, \qquad \text{(per engine)} \tag{1}$$

in which $\dot{w}_{f,0}$ is the basic fuel flow rate (without shaft-power extraction) for each of $N_{op,eng}$ engines which are assumed to contribute equally to the total shaft-power P_{spx}. The constant k_p^* was given as $k_p^* = 0.0094$ N/W as an average of the penalties computed at flight altitudes of 0 ft, 10,000 ft, 20,000 ft, and 35,000 ft at Mach numbers of 0.30, 0.60, and 0.85 at maximum continuous thrust [42]. The incremental fuel flow $\Delta\dot{w}_{f,bx}$ due to bleed air extraction $\dot{w}_{bld} = \dot{m}_{bld} \cdot g$ per engine is computed following the method of SAE AIR 1168/8 [43] as

$$\Delta\dot{w}_{f,bx} = 0.0335\ \left(\frac{T_{tet}[^\circ R]}{2000}\ \frac{\dot{w}_{bld}}{N_{op,eng}}\right), \qquad \text{(per engine)} \tag{2}$$

in which T_{tet} is the turbine entry temperature, for which a representative value of 2,400°R is used in this paper. Off-take penalty relationships such as Eq. 1 and Eq. 2 are useful as they require little information other than the time variation of the shaft-power and bleed air off-takes. They are, however, general relationships that do not account for the effect of the engine cycle parameters on the engine's sensitivity to secondary power extraction. The effect of this uncertainty on the performance of a substantially electrified subsystem architecture relative to a conventional one is assessed through a factor κ_{spp} that modifies the secondary power extraction penalty relationships shown above. Of particular interest is a case where shaft-power extraction is *more* expensive than predicted by Eq. 1 and bleed extraction is *less* expensive than predicted by Eq. 2. This scenario is modeled as follows: (i) the factor κ_{spp} is constrained as $\kappa_{spp} \geq 0$, (ii) the RHS of Eq. 1 is multiplied by the quantity $(1 + \kappa_{spp})$, and (iii) the RHS of Eq. 2 is multiplied by the quantity $(1 - \kappa_{spp})$.

From Fig. 9 ($\kappa_{spp} = 0.5$), it is evident that the results, in terms of architecture composition, are very sensitive to the secondary power extraction penalties. Here, since shaft-power off-take becomes relatively more expensive and bleed air off-take simultaneously becomes relatively less

expensive, a pneumatic ECS solution is favored across the entire population. The appearance of pneumatic WIPS and CIPS solutions within the Pareto bands is observed as well. Further, since shaft-power off-take is more expensive, the proportion of architectures with electrified actuation functions increases, since these are power-on-demand (and there is no power draw associated with leakage flow). Another important observation is that trends in the aircraft-level continuous design variables for the non-dominated solutions remain largely unchanged, implying that the subsystem architecture has a somewhat more significant impact on the objectives for these scenarios.

The architecture composition and continuous aircraft-level design variable variations within the Pareto bands also depends on the choice of the objective functions. Figure 10 shows the results of multi-objective optimization with OEW and BF as objective functions. An interesting observation is that unlike in Fig. 8, Fig. 10 shows a split discontinuous Pareto frontier when the objective functions are OEW and BF. Another difference is the presence of pneumatic ECS (0) in addition to electric ECS (1) in the composition of architectures. Inspection revealed that electric ECS designs were located in the disconnected cluster of points with low BF but higher OEW. This is a consequence of fuel savings achieved by a nevertheless heavier electric ECS architecture. Unlike in Fig. 8, where

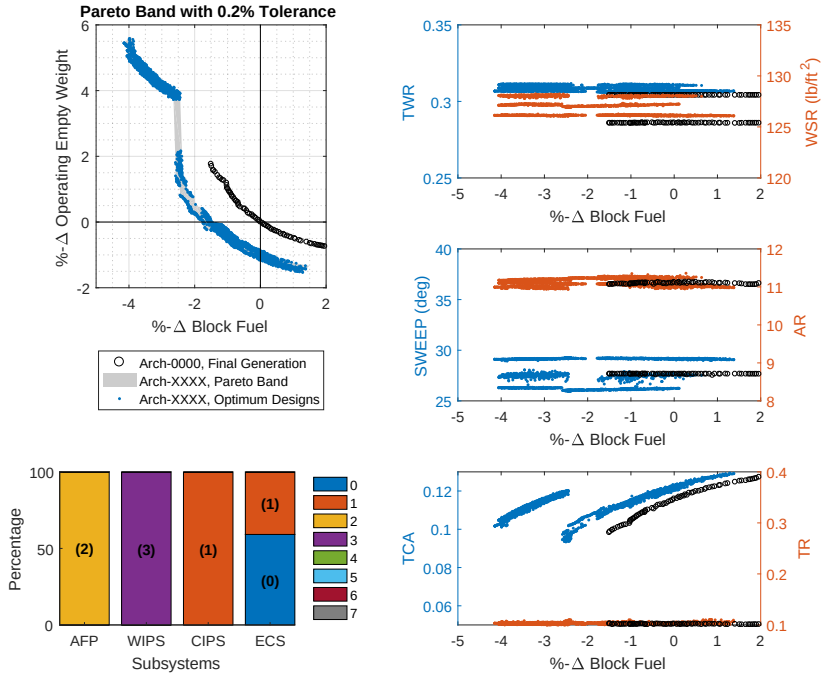

Fig. 10 Variation of SSA OEW, BF, and design variables within Pareto band

increasing fuel savings occurred for lower thrust-to-weight designs, Fig. 10 shows no significant variation of thrust-to-weight within the Pareto band. Since the TOFL is no longer an objective, the thrust-to-weight ratio is driven down as far as permitted by SSFOR and AMFOR performance constraints.

C. Large Twin-Aisle Aircraft

Figure 11 shows the movement of the LTA TOFL, BF Pareto frontiers and the composition of subsystem architectures (in percentages) with successive generations. It is evident that

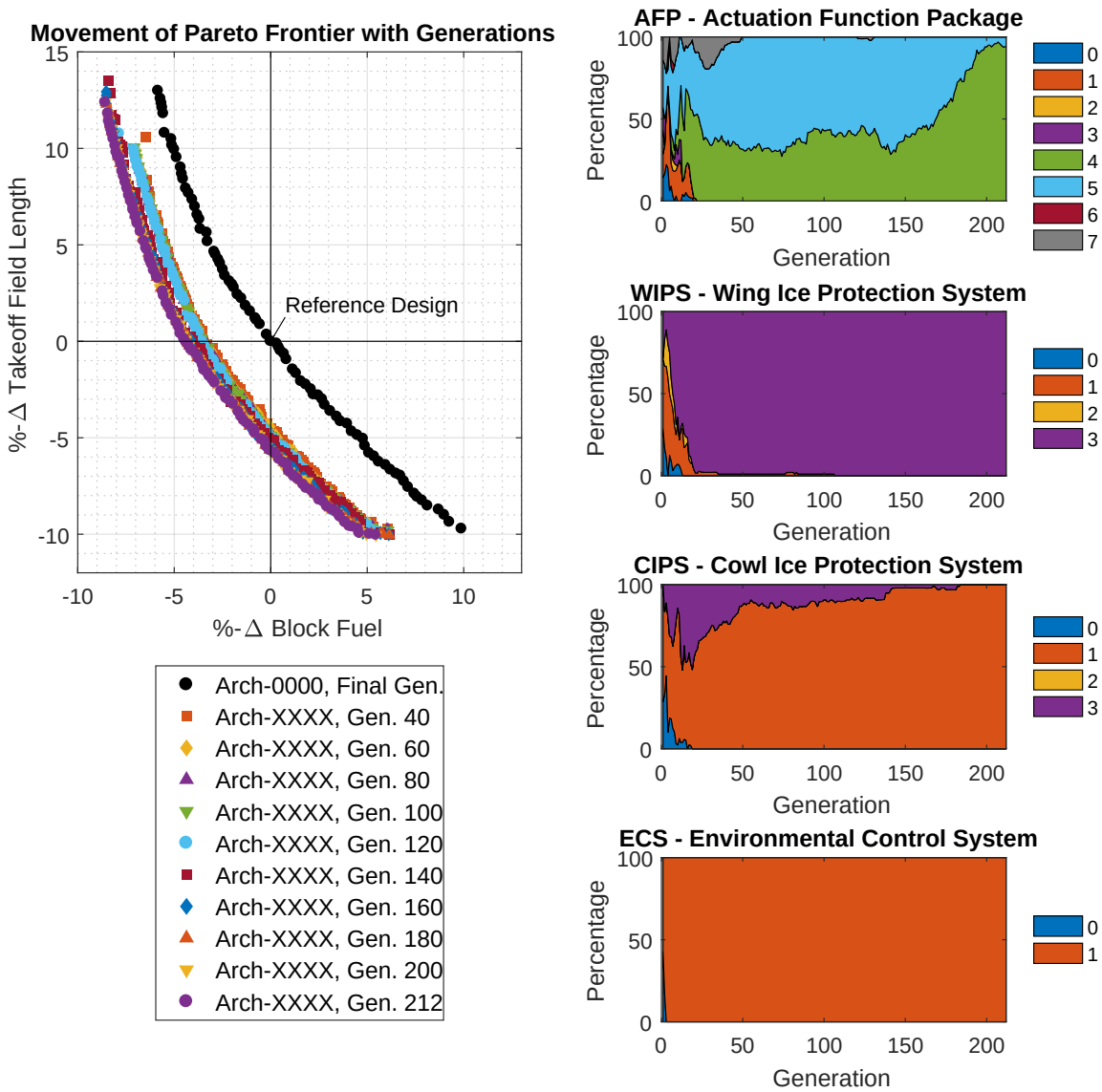

Fig. 11 Evolution (over generations) of LTA BF, TOFL, and architecture compositions on Pareto Frontiers

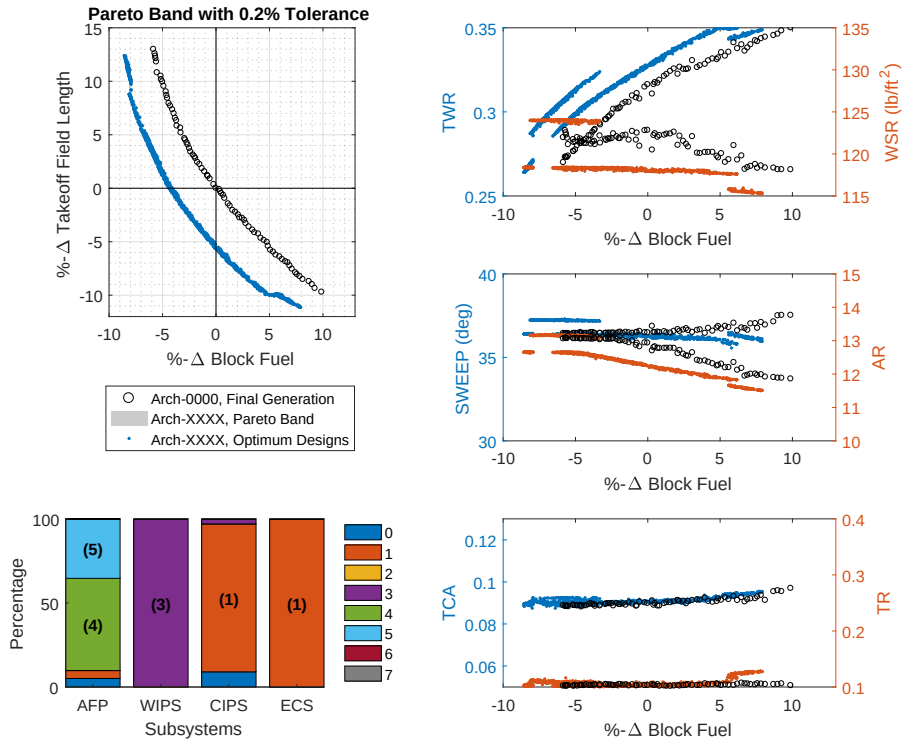

Fig. 12 Variation of LTA TOFL, BF, and design variables within Pareto band

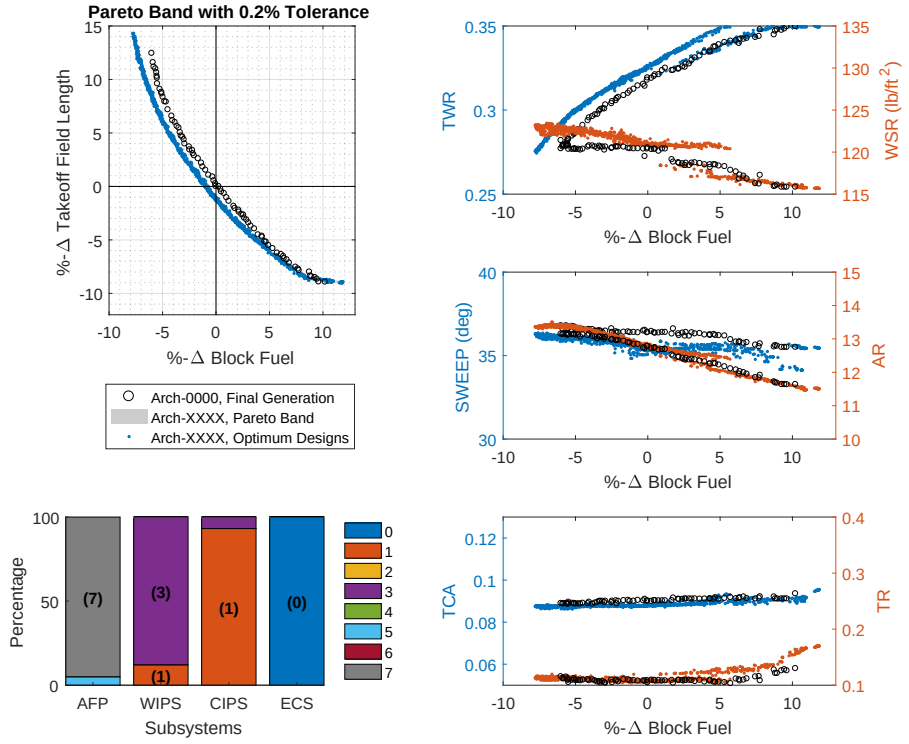

Fig. 13 Variation of LTA TOFL, BF, and design variables within Pareto band, $\kappa_{spp} = 0.5$

non-dominated designs feature substantially electrified actuation (AFP#-4 and -5), electrothermal

running-wet de-icing WIPS (WIPS descriptor = 3), pneumatic running-wet anti-icing CIPS (CIPS descriptor = 1), and electric ECS (ECS descriptor = 1). Similar to the case of the SSA, dominant architectures emerge at fairly early generations, with most of the optimization in later generations being driven by the aircraft-level continuous design variables.

When the sensitivity to secondary power extraction penalties is assessed with a setting of $\kappa_{spp} = 0.5$, the ECS architecture reverts to pneumatic throughout the Pareto band (ECS descriptor = 0), as depicted in Fig. 13 (similar to the SSA case). The threshold value of κ_{spp} at which the ECS architecture reverts from electric to pneumatic was found to be higher for the LTA than for the SSA. This observation implies that the LTA is relatively less sensitive to the factor κ_{spp}, due to the comparatively larger contribution of ECS bleed air off-take to the total fuel impact for the larger, longer-range LTA. When the objectives are changed to OEW and BF as shown in Fig. 14, a disconnected Pareto band is seen similar to that for the SSA (with largely similar observations regarding architecture composition).

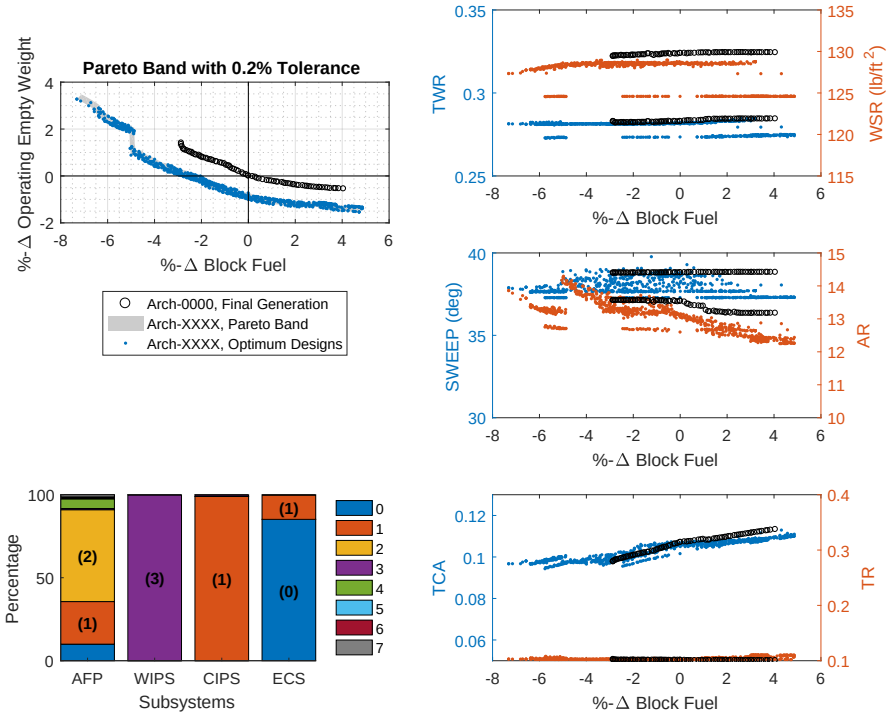

Fig. 14 Variation of LTA EW, BF continuous and discrete design variables within Pareto band

VI. Conclusion and Future Work

This work presented a multi-objective constrained optimization approach for aircraft sizing taking into account the impact of the major aircraft subsystems. The approach uses the Non-Dominated Sorting Algorithm II (NSGA-II) to harness the Integrated Subsystem Sizing and Architecture Assessment Capability (ISSAAC) framework, using both continuous design variables for key aircraft-level design parameters and discrete variables as subsystem architecture descriptors. For both a Small Single-aisle Aircraft (SSA) and a Large Twin-aisle Aircraft (LTA), successive generations revealed the evolution of architecture composition on the Pareto frontier towards a small number of dominant subsystem architectures. For both aircraft, these architectures involved electrification of the Environmental Control System (ECS), which occurred in early generations of the optimization and had a significant impact. Electrothermal de-icing solutions for the Wing Ice Protection System (WIPS) were also found to be dominant, while pneumatic running-wet anti-icing solutions dominated for the Cowl Ice Protection System (CIPS). The dominant architectures for the two aircraft sizes showed varying levels of electrification for the actuation functions. The architecture composition within the Pareto bands (generated by a look-back starting from the final Pareto frontiers) changed significantly when the magnitudes of thrust-specific fuel consumption degradation arising from shaft-power and bleed air extraction were varied in opposite directions. In particular, when shaft-power extraction was made relatively more expensive and bleed air extraction relatively less expensive, the electrification trends observed for ECS, in particular, were reversed. The results of this paper show that while it may be possible to decouple subsystem-related impacts from configuration-level design work for conventional subsystem architectures, this is not appropriate when unconventional (e.g., More Electric) subsystem architectures are permitted or considered. Among the strengths of the developed approach is the explicit consideration of subsystem architecture impacts, automated investigation of subsystem architecture design space, largely physics-based modeling and sizing of novel subsystem architecture components, preliminary calculation of fuel consumption penalties due to secondary power extraction, multi-objective optimization setup to assess performance with respect to competing objective functions, and Genetic Algorithm usage to handle combination of discrete and continuous design variables. Though not one of the major thrusts of the current work,

the incorporation of proprietary/manufacturers' data or methods regarding the subsystem architecture (to replace the currently used public domain data and models) will enhance the practical applicability of the demonstrated approach. Avenues for future work include (i) formulation of a larger scale optimization problem in which optimization is also performed at the subsystems-level and (ii) a formal assessment of the impact of propagating epistemic and technological uncertainty on the results of such multi-objective optimization problems.

References

[1] Henderson, R. P., Martins, J., and Perez, R. E., "Aircraft conceptual design for optimal environmental performance," *Aeronautical Journal*, Vol. 116, No. 1175, 2012, pp. 1, url: https://doi.org/10.1017/S000192400000659X.

[2] Antoine, N. E. and Kroo, I. M., "Framework for aircraft conceptual design and environmental performance studies," *AIAA journal*, Vol. 43, No. 10, 2005, pp. 2100–2109, url: https://doi.org/10.2514/1.13017.

[3] Cabral, L. V., Paglione, P., and Mattos, B., "Multi-objective design optimization framework for conceptual design of families of aircraft," *44th AIAA Aerospace Sciences Meeting and Exhibit, Reno, Nevada*, 2006, pp. 2006–1328, url: https://doi.org/10.2514/6.2006-1328.

[4] Daskilewicz, M. J., German, B. J., Takahashi, T. T., Donovan, S., and Shajanian, A., "Effects of disciplinary uncertainty on multi-objective optimization in aircraft conceptual design," *Structural and Multidisciplinary Optimization*, Vol. 44, No. 6, 2011, pp. 831–846, url: https://doi.org/10.1007/s00158-011-0673-4.

[5] Ilario da Silva, C. R., Orra, T. H., and Alonso, J. J., "Multi-Objective Aircraft Design Optimization for Low External Noise and Fuel Burn," *58th AIAA/ASCE/AHS/ASC Structures, Structural Dynamics, and Materials Conference*, 2017, p. 1755, url: https://doi.org/10.2514/6.2017-1755.

[6] Sinnett, M., "Boeing 787 No-Bleed Systems: Saving Fuel and Enhancing Operational Efficiencies," Boeing Aero Magazine, Quarter 4, Online: http://www.boeing.com/commercial/aeromagazine/, 2007.

[7] Nelson, T., "787 Systems and Performance," Flight Operations Engineering, Boeing Commercial Airplanes, March 2009, online: http://myhres.com/Boeing-787-Systems-and-Performance.pdf, accessed November 4, 2015.

[8] Van den Bossche, D., "The A380 Flight Control Electrohydrostatic Actuators, Achievements and Lessons Learnt," *25th International Congress of the Aeronautical Sciences, ICAS 2006*, Hamburg, Germany,

2006, url: http://icas.org/ICAS_ARCHIVE/ICAS2006/PAPERS/048.PDF.

[9] Jones, R., "The More Electric Aircraft: the past and the future?" *IEE Colloquium on Electrical Machines and Systems for the More Electric Aircraft*, 1999, pp. 1/1–1/4, url: https://doi.org/10.1049/ic:19990830.

[10] Cronin, M., "The all-electric aircraft," *IEE Review*, Vol. 36, No. 8, sep 1990, pp. 309 –311, url:https://doi.org/10.1049/ir:19900132.

[11] Chakraborty, I. and Mavris, D., "Integrated Assessment of Aircraft and Novel Subsystem Architectures in Early Design," *AIAA Science and Technology Exposition and Forum (SciTech)*, No. AIAA 2016-0215, San Diego, California, 4-8 January 2016, url: https://doi.org/10.2514/6.2016-0215.

[12] Raymer, D., *Aircraft Design: A Conceptual Approach*, AIAA Education Series, 5th ed., 2012, url: https://doi.org/10.2514/4.869112.

[13] Roskam, J., *Airplane Design Part V - Component Weight Estimation*, Design Analysis & Research, 1999.

[14] Torenbeek, E., *Synthesis of Subsonic Airplane Design: An Introduction to the Preliminary Design of Subsonic General Aviation and Transport Aircraft, with Emphasis on Layout, Aerodynamic Design, Propulsion and Performance*, Delft University Press, 1976, url: https://doi.org/10.1007/978-94-017-3202-4.

[15] Chakraborty, I. and Mavris, D. N., "Integrated Assessment of Aircraft and Novel Subsystem Architectures in Early Design," *54th AIAA Aerospace Sciences Meeting*, 2016, p. 0215, url: https://doi.org/10.2514/6.2016-0215.

[16] Chakraborty, I. and Mavris, D. N., "Assessing Impact of Epistemic and Technological Uncertainty on Aircraft Subsystem Architectures," *16th AIAA Aviation Technology, Integration, and Operations Conference*, 2016, p. 3145, url: https://doi.org/10.2514/6.2016-3145.

[17] Lammering, T., *Integration of Aircraft Systems into Conceptual Design Synthesis*, Ph.D. thesis, Institute of Aeronautics and Astronautics (ILR), RWTH Aachen University, 2014.

[18] Deb, K., *Multi-objective optimization using evolutionary algorithms*, Vol. 16, John Wiley & Sons, 2001.

[19] Deb, K., Pratap, A., Agarwal, S., and Meyarivan, T., "A fast and elitist multiobjective genetic algorithm: NSGA-II," *IEEE transactions on evolutionary computation*, Vol. 6, No. 2, 2002, pp. 182–197, url: https://doi.org/10.1109/4235.996017.

[20] Chakraborty, I., *Subsystem Architecture Sizing and Analysis for Aircraft Conceptual Design*, Ph.D. thesis, Daniel F. Guggenheim School of Aerospace Engineering, Georgia Institute of Technology, Atlanta, GA, USA, Online: https://smartech.gatech.edu/handle/1853/54427, December 2015.

[21] Chakraborty, I. and Mavris, D. N., "Integrated Assessment of Aircraft and Novel Subsystem Architectures in Early Design," *Journal of Aircraft*, 2016, pp. 1–15, url: https://doi.org/10.2514/1.C033976.

[22] Sanchis, J., Martinez, M., Blasco, X., and Salcedo, J., "A new perspective on multiobjective optimization by enhanced normalized normal constraint method," *Structural and multidisciplinary optimization*, Vol. 36, No. 5, 2008, pp. 537–546, url: https://doi.org/10.1007/s00158-007-0185-4.

[23] Messac, A., Ismail-Yahaya, A., and Mattson, C. A., "The normalized normal constraint method for generating the Pareto frontier," *Structural and multidisciplinary optimization*, Vol. 25, No. 2, 2003, pp. 86–98, url: https://doi.org/10.1007/s00158-002-0276-1.

[24] Das, I. and Dennis, J. E., "Normal-boundary intersection: A new method for generating the Pareto surface in nonlinear multicriteria optimization problems," *SIAM Journal on Optimization*, Vol. 8, No. 3, 1998, pp. 631–657, url: https://doi.org/10.1137/S1052623496307510.

[25] McCullers, L., *Flight Optimization System, Release 8.11, User's Guide*, NASA Langley Research Center, Hampton, VA 23681-0001, October 9 2009.

[26] Lytle, J. K., "The Numerical Propulsion System Simulation: An Overview," NASA/TM-2000-209915, http://ntrs.nasa.gov/archive/nasa/casi.ntrs.nasa.gov/20000063377.pdf, June 2000.

[27] Chakraborty, I. and Mavris, D., "Heuristic Definition, Evaluation, and Impact Decomposition of Aircraft Subsystem Architectures," *AIAA Aviation 2016 Conference*, No. AIAA-2016-3144, Washington D.C., June 13-17, 2016, url: https://doi.org/10.2514/6.2016-3144.

[28] Roskam, J., *Airplane Design Part VI - Preliminary Calculation of Aerodynamic, Thrust and Power Characteristics*, Design Analysis & Research, 1999.

[29] Scholz, D., "Development of a CAE-Tool for the Design of Flight Control and Hydraulic Systems," *AeroTech '95*, Birmingham, U.K., 1995.

[30] "Federal Aviation Regulations (FAR) Part 25 - Airworthiness Standards: Transport Category Airplanes," Federal Aviation Administration (FAA), online: http://www.ecfr.gov/, accessed November 4, 2015.

[31] Simsic, C., "Electric actuation system duty cycles," *Aerospace and Electronics Conference, 1991. NAECON 1991., Proceedings of the IEEE 1991 National*, 1991, pp. 540–545 vol.2.

[32] *Boeing 777 Aircraft Maintenance Manual, Chapter 27 - Flight Controls*, 2006.

[33] Society of Automotive Engineers, "SAE Aerospace Information Report (AIR) 5005A - Commercial Aircraft Hydraulic Systems," 2010.

[34] Socheleau, J., Mare, J.-C., and Baudu, P., "Actuation Technologies and Application - Flight Controls and Thrust Reverser Actuation," *Technologies for Energy Optimized Aircraft Equipment Systems*

(TEOS forum), Paris, France, 2006.

[35] Chakraborty, I., Mavris, D., Emeneth, M., and Schneegans, A., "An Integrated Approach to Vehicle and Subsystem Sizing and Analysis for Novel Subsystem Architectures," *Proc IMechE Part G: J Aerospace Engineering*, Vol. 230, No. 3, 2016, pp. 496–514, url: https://doi.org/10.1177/0954410015594399.

[36] Cameron-Johnson, A., "Some Aspects of the Design of Aircraft Steering Systems," *Aircraft Engineering and Aerospace Technology*, Vol. 43, No. 6, 1971, pp. 7–10, url: https://doi.org/10.1108/eb034778.

[37] Bennett, J., Mecrow, B., Atkinson, D., Maxwell, C., and Benarous, M., "Fault-tolerant electric drive for an aircraft nose wheel steering actuator," *IET Electrical Systems in Transportation*, Vol. 1, No. 3, 2011, pp. 117–125, url: https://doi.org/10.1049/iet-est.2010.0054.

[38] Collins, A., "EABSYS: Electrically Actuated Braking System," *IEE Colloquium on Electrical Machines and Systems for the More Electric Aircraft*, London, U.K., 1999, p. 4, url: https://doi.org/10.1049/ic:19990833.

[39] Scholz, D., "MPC 75 Hydraulic Load Analysis," Technical Note TN-EV52-362/91, Deutsche Airbus, Hamburg, July 1991.

[40] Herzog, J., "Electrification of the Environmental Control System," *25th International Congress of the Aeronautical Sciences (ICAS)*, No. ICAS 2006-7.7.1, Hamburg, Germany, 3 - 8 September 2006, url: http://icas.org/ICAS_ARCHIVE/ICAS2006/PAPERS/344.PDF.

[41] Meier, O. and Scholz, D., "A Handbook Method for the Estimation of Power Requirements for Electrical De-Icing Systems," *Deutscher Luft-und Raumfahrtkongress 2010*, Hamburg, Germany, Aug. 31 - Sept. 2 2010, url: http://www.mp.haw-hamburg.de/pers/Scholz/MOZART/MOZART_PUB_DLRK_10-08-31.pdf.

[42] Scholz, D., Seresinhe, R., Staack, I., and Lawson, C., "Fuel Consumption due to Shaft Power Off-takes from the Engine," *4th International Workshop on Aircraft System Technologies, AST 2013*, Shaker, Hamburg,, April 23-24 2013, pp. 169–179, url: https://pdfs.semanticscholar.org/5fb0/836dac3bcec4c32847c7cb193c1e3e1c52fd.pdf.

[43] Society of Automotive Engineers, "SAE Aerospace Applied Thermodynamics Manual - SAE AIR 1168," 1989.